4738 *Biochemistry* **2009,** *48,* 4738–4746
DOI: 10.1021/bi900118j

BIOCHEMISTRY
including biophysical chemistry & molecular biology
Article

Evidence for Heme Oxygenase Activity in a Heme Peroxidase[†,‡]

Sandip K. Badyal,[§] Graham Eaton,[§] Sharad Mistry,[∥] Zoi Pipirou,[§] Jaswir Basran,[⊥] Clive L. Metcalfe,[§] Andrea Gumiero,[§] Sandeep Handa,[§] Peter C. E. Moody,[⊥] and Emma Lloyd Raven*[,§]

[§]*Department of Chemistry, Henry Wellcome Building, University of Leicester, University Road, Leicester LE1 7RH, U.K.,* [∥]*Protein and Nucleic Acid Chemistry Laboratory, University of Leicester, Lancaster Road, Leicester LE1 9HN, U.K., and* [⊥]*Department of Biochemistry and Henry Wellcome Laboratories for Structural Biology, Henry Wellcome Building, University of Leicester, Lancaster Road, Leicester LE1 9HN, U.K.*

Received November 18, 2008. Revised Manuscript Received March 22, 2009

ABSTRACT: The heme peroxidase and heme oxygenase enzymes share a common heme prosthetic group but catalyze fundamentally different reactions, the first being H_2O_2-dependent oxidation of substrate using an oxidized Compound I intermediate, and the second O_2-dependent degradation of heme. It has been proposed that these enzymes utilize a common reaction intermediate, a ferric hydroperoxide species, that sits at a crossroads in the mechanism and beyond which there are two mutually exclusive mechanistic pathways. Here, we present evidence to support this proposal in a heme peroxidase. Hence, we describe kinetic data for a variant of ascorbate peroxidase (W41A) which reacts slowly with *tert*-butyl hydroperoxide and does not form the usual peroxidase Compound I intermediate; instead, structural data show that a product is formed in which the heme has been cleaved at the α-*meso* position, analogous to the heme oxygenase mechanism. We interpret this to mean that the Compound I (peroxidase) pathway is shut down, so that instead the reaction intermediate diverts through the alternative (heme oxygenase) route. A mechanism for formation of the product is proposed and discussed in the light of what is known about the heme oxygenase reaction mechanism.

Heme oxygenase (HO)[1] catalyzes the degradation of heme in biological systems (*1*−*7*). It does this by means of an oxygen-dependent reaction mechanism that converts heme, sequentially, to α-*meso*-hydroxyheme, verdoheme, and biliverdin, a reaction that releases both CO and free iron (Scheme 1). The CO released during HO catalysis might well be coupled to other biological processes, because CO is one of a few small, gaseous molecules that are thought to have a signaling role *in vivo* (*8*−*10*).

The initial step of the HO mechanism involves one-electron reduction of a ferrous−oxy heme species to give a ferric hydroperoxide intermediate, followed by formation of α-*meso*-hydroxyheme. Reaction of hydrogen peroxide (O_2^{2-}) with the ferric form of the enzyme, to form the same ferric−hydroperoxide intermediate, can also catalyze this first step (*11*−*18*). The conversion of verdoheme to biliverdin was initially believed to be catalyzed only by reaction with oxygen (*1*,*11*), but it is now known that hydrogen peroxide and its derivative MeO_2H can substitute for oxygen in this reaction, too (*19*,*20*).

There is an obvious similarity here between the heme oxygenase reaction mechanism and that of the related heme peroxidase enzymes, both of which use a transient ferric hydroperoxide intermediate. There are differences though. In the peroxidases, the ferric−peroxide intermediate is not normally observed because its decay to an oxidized Compound I intermediate occurs more rapidly than its formation. Accordingly, no evidence for heme oxygenase reactivity has been observed for a peroxidase enzyme. In contrast, the ferric hydroperoxide intermediate in heme oxygenase converts to α-*meso*-hydroxyheme and does not form an oxidized Compound I species. Indeed, in cases where reaction of HO with different peroxides (such as *m*-chloroperoxybenzoic acid, *tert*-butyl hydroperoxide, and cumene peroxide) leads to formation of a Compound I, no heme degradation is observed (*11*,*21*). Together, the consensus of data from the HO work has led to the suggestion (*3*,*4*,*7*) that HO and the heme peroxidase enzymes share a common reaction intermediate, the ferric hydroperoxide species, but that the two routes for decay of the intermediate are mutually exclusive (Scheme 2).

Up to now, there has been no experimental evidence from studies on peroxidase enzymes to support this proposal. In this work, we have studied a variant of ascorbate

[†]This work was supported by grants from the BBSRC (studentship to S.K.B.). ESRF Awards MX606 and MX635 funded the beam-time and microspectrophotometry.

[‡]PDB accession code for the protein structure reported in this paper is 2WD4 (W41A variant soaked in *t*-BuOOH).

*To whom correspondence should be addressed. Telephone: +44 (0)116 2297047. Fax: +44 (0)116 2522789. E-mail: emma.raven@le.ac.uk.

[1]Abbreviations: APX, ascorbate peroxidase; HO, heme oxygenase; *t*-BuOOH, *tert*-butyl hydroperoxide.

 Published on Web 03/23/2009

Scheme 1: Overall Reaction Catalyzed by HO

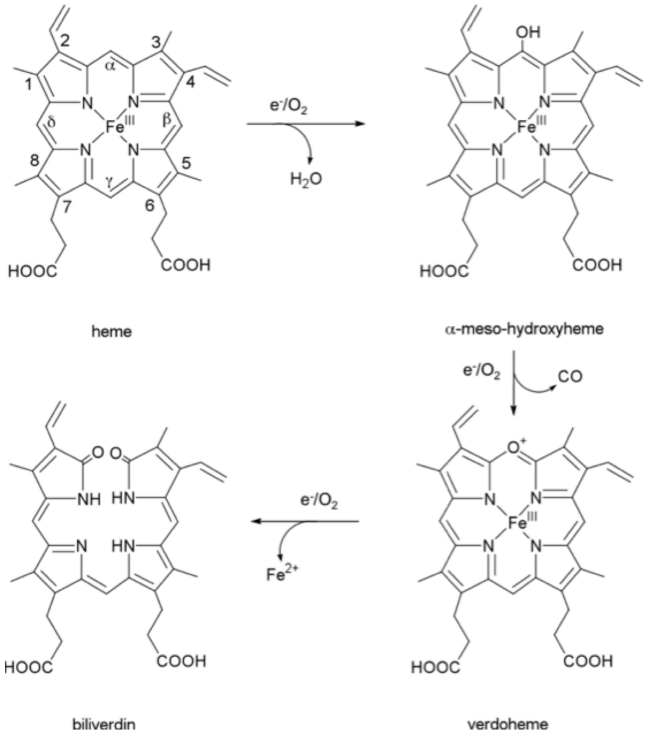

Scheme 2: Decay of the Ferric Hydroperoxide Intermediate, either to α-*meso*-Hydroxyheme, as in HO, or to Compound I, as in the Heme Peroxidases (as Well as the P450s and Nitric Oxide Synthase)[a]

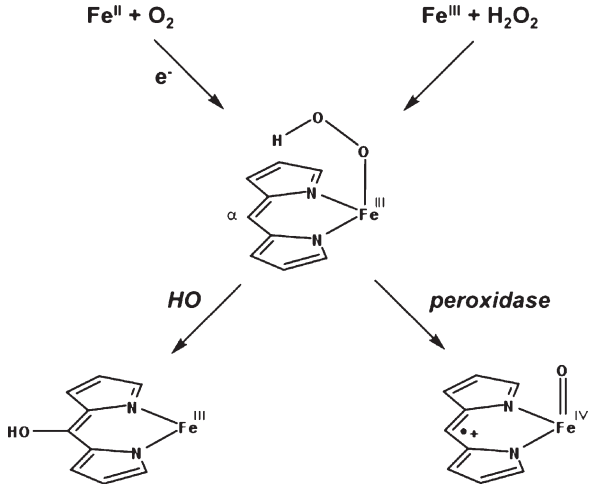

[a] Adapted from ref 7.

peroxidase (W41A) which is known (*22*) to react slowly with peroxide on account of a mobile distal ligand (His42) that moves on and off the iron during the reaction. Here, we show that formation of Compound I does not occur in this variant on reaction with *tert*-butyl hydroperoxide. Instead, the reaction is diverted through the alternative route, leading to formation of a degraded heme product that is cleaved at the α-*meso* position. To our knowledge, this is the first time that heme cleavage has been observed crystallographically in a peroxidase enzyme, and the data provide evidence for a common reaction intermediate in the two enzymes. A mechanism for this reaction is proposed and discussed in terms of the known chemistry of the HO reaction mechanism.

EXPERIMENTAL PROCEDURES

Materials. L-Ascorbic acid (Aldrich, ε_{290} = 2.8 mM^{-1} cm^{-1}) (*23*) and the chemicals used for buffers were of the highest analytical grade (more than 99% pure) and were used without further purification. α-Cyano-4-hydroxycinnamic acid was purchased from Fluka. Hydrogen peroxide solutions were freshly prepared by dilution of a 30% (v/v) solution (BDH Chemicals); exact concentrations were determined using the published absorption coefficient (ε_{240} = 39.4 M^{-1} cm^{-1}) (*24*). Solutions of *t*-BuOOH were freshly prepared by dilution of a 70% (v/v) solution (Avocado Research Chemicals). Aqueous solutions were prepared using water purified through an Elgastat Option 2 water purifier, which itself was fed with deionized water. All pH measurements were made using a Russel pH electrode attached to a digital pH meter (Radiometer Copenhagen, model PHM 93). All molecular biology kits and enzymes were used according to manufacturer's protocols.

Protein Expression and Purification. Bacterial fermentation of cells and purification of wild-type APX and W41A were carried out according to published procedures (*22*,*25*). Purified samples of wild-type APX and W41A showed wavelength maxima at 407, 525, and ≈630 nm and 405, 525, and ≈630 nm, respectively, as reported previously (*22*,*26*). Enzyme concentrations for wild-type APX and W41A were determined using absorption coefficients of ε_{407} = 107 mM^{-1} cm^{-1} (*26*) and ε_{405} = 125 mM^{-1} cm^{-1} (*22*), respectively.

Electronic Absorption Spectroscopy and Kinetics. Electronic absorption spectra were collected using a Perkin-Elmer Lambda 35 spectrophotometer, linked to a PC workstation running UV-Winlab software.

Transient-state measurements were performed using an SX.18MV microvolume stopped-flow spectrophotometer (Applied Photophysics) fitted with a Neslab RTE-200 circulating water bath (5 ± 0.1 °C). Reported values of k_{obs} are an average of at least five measurements. Individual traces were monophosic in all cases. All kinetic data were analyzed using nonlinear least-squares regression analysis on an Archimedes 410-1 microcomputer (Applied Photophysics) using Spectrakinetics software. All curve fitting was performed using the Grafit 5 software package (Grafit version 5.0.3, Erithacus Software Ltd.). Formation of Compound I ($k_{1,obs}$) was monitored at the wavelength maximum for the ferric enzyme by mixing enzyme (2 μM) with various concentrations of *t*-BuOOH.

Multiple-wavelength absorption studies were carried out using a photodiode array detector and X-SCAN software (Applied Photophysics Ltd.). Spectral deconvolution was performed by global analysis and numerical integration methods using PROKIN software (Applied Photophysics Ltd.). To ensure consistency with the crystallographic data, all experiments were carried out in sodium phosphate buffer (pH 8.3, μ = 0.1 M), but in

control experiments using sodium phosphate buffer (pH 7.0, μ = 0.1 M) or crystal screen buffers (0.1 M Hepes, pH 8.3, 2.25 M lithium sulfate) identical results were obtained.

Structure Identification and Structure Determination. Crystals of W41A were obtained using previously published procedures (*27*). The *t*-BuOOH-soaked W41A structure was obtained by soaking crystals for 15 min in a fresh solution of *t*-BuOOH (72.5 mM) made up in mother liquor (0.1 M Hepes (pH 8.3) and 2.25 M lithium sulfate). We tried numerous other soaks of different durations (5, 10, 15 min) for both wild-type and W41A crystals with various concentrations of both hydrogen peroxide and *t*-BuOOH (up to ~100 mM). In none of these cases was it possible to obtain crystallographic information for the final product. All crystals were flash-frozen and then cryocooled in liquid nitrogen and stored for data collection. High performance liquid chromatography and MALDI-Tof and electrospray ionization mass spectrometry were used for product identification in solution.

All Synchrotron data were collected at 100 K at the ESRF, Grenoble. Diffraction data for *t*-BuOOH-soaked W41A was collected using beamline ID14-1 and an ADSC Q210 CCD detector. The data were indexed and scaled using MOSFLM (*28*) and SCALA (*29*). Crystals were continuously cooled by a cold nitrogen stream from an Oxford Cryosystems 700 series cryostream. Single-crystal microspectrometry measurements from the *t*-BuOOH-soaked W41A crystals were taken before and after X-ray data collection. UV−visible absorption spectra of the crystals in the 500−800 nm range were recorded at ESRF (beamline ID14-2) using the EMBL online microspectrophotometer (HR2000 CCD detector, Ocean Optics). Input light was provided by a deuterium/halogen source (Ocean Optics, DH2000) coupled to custom lenses via a 100 μm 2-UV-SR fiber optic (generating a focal spot of 25 μm) and collected from the second lens coupled to a 600 μm fiber optic. Spectra were recorded at the same ϕ position. The spectrum of the cryocooled crystals remained unchanged during storage.

Data collection and processing statistics are shown in Table 1; 5% of the data were flagged for the calculation of R_{free} and excluded from subsequent refinement. The *t*-BuOOH-soaked W41A structure was refined from the 1.35 Å ferric W41A structure (PDB code 2GGN) (*22*). The modified heme porphyrin in *t*-BuOOH-soaked W41A was based on the 2.19 Å iron-free biliverdin structure from human HO (PDB code 1S8C) (*30*). The dictionary for refinement was constructed with the program SKETCHER in the CCP4 suite (*35*). Several cycles of refinement using REFMAC5 (*31*) from the CCP4 suite (*29*) and manual rebuilding of the protein model using COOT (*32*) followed by the addition of water molecules were carried out until the R_{free} and R_{factor} values converged. The structure and diffraction data were deposited with the following identifier: PDB code 2WD4. The final refinement statistics are presented in Table 1.

Table 1: Data Collection and Refinement Statistics[a]

Data Collection	
resolution (Å)	82.20−1.40 (1.48−1.40)
total observations	386646 (51240)
unique reflections	51023 (7330)
$\langle I\rangle/\langle\sigma I\rangle$	16.5 (3.7)
R_{merge}	0.06 (0.57)
completeness (%)	100 (100)
Refinement	
R_{factor}	0.189
R_{free}	0.217
rmsd from ideal	
angles (deg)	1.62
bonds (Å)	0.008

[a] Values in parentheses are for the outer shell.

RESULTS

Reaction with tert-Butyl Hydroperoxide. The reactions of both wild-type APX (Figure 1A,B) and W41A (Figure 1C,D) with *t*-BuOOH (Figure 1A,C) and H_2O_2 (Figure 1B,D) were monitored spectrophotometrically over 15 min. For the W41A variant, a rapid decrease of the absorbance at the Soret maxima and the α and β bands was observed on reaction with *t*-BuOOH (Figure 1C) and accompanied by a change in color from red to green (Supporting Information Figure S1). In contrast to the wild-type protein (Figure 1A), no evidence for formation of a ferryl species was detected under any conditions for W41A. At the end of the reaction, the final product in solution shows maxima in the visible region (λ_{max}/nm = 405, 532, 564, 630 nm, Figure 1C) which are similar to the final spectrum obtained when a crystal of W41A is soaked in the same peroxide (Figure 4, see below). Similar spectroscopic changes are observed when HO is reacted with H_2O_2 (*11*,*14*,*17*,*18*,*33*), although in HO an increase in absorbance at ~700 nm is observed, indicative of verdoheme formation, which is not observed for W41A on this time scale. The corresponding spectra on reaction of W41A with H_2O_2 are shown for comparison (Figure 1D). The reactivity of W41A with *t*-BuOOH and the failure to form a distinct Compound I intermediate are consistent with previous work in which this variant has been shown (*22*) to react more slowly with H_2O_2 than the wild-type protein, although it still forms distinct Compound I and II intermediates (accordingly, there is no evidence for heme degradation on reaction of W41A with H_2O_2).

In control experiments over identical time scales (spectrophotometrically; Figure 1) and faster (using stopped flow; data not shown), we showed that wild-type APX reacts normally with *t*-BuOOH (Figure 1A) and that formation of Compound I occurs as expected (λ_{max}/nm = 410, 530, 570 (sh), and 650) but is slower (k_1 = (9.7 ± 0.5) × 10^4 M^{-1} s^{-1}) than for the equivalent H_2O_2 reaction (k_1 = (3.3 ± 0.1) × 10^7 M^{-1} s^{-1} (*34*)). Furthermore, formation ($k_{2,t\text{-BuOOH}}$ = 2.1 ± 0.1 s^{-1}) of Compound II (λ_{max}/nm = 414, 527, and 560 (sh)) follows normally as a first-order decay process (compare $k_{2,HOOH}$ = 2.7 ± 0.1 s^{-1} (*34*)). The spectra for wild-type APX on reaction with H_2O_2 are shown for comparison (Figure 1B). No evidence for heme degradation was observed for wild-type APX with either H_2O_2 (Figure 1B) or *t*-BuOOH (Figure 1A).

In photodiode array stopped-flow experiments over faster time scales (1.28−500 ms), no evidence for formation of a transient Compound I intermediate on reaction of W41A with *t*-BuOOH was observed (data not shown),

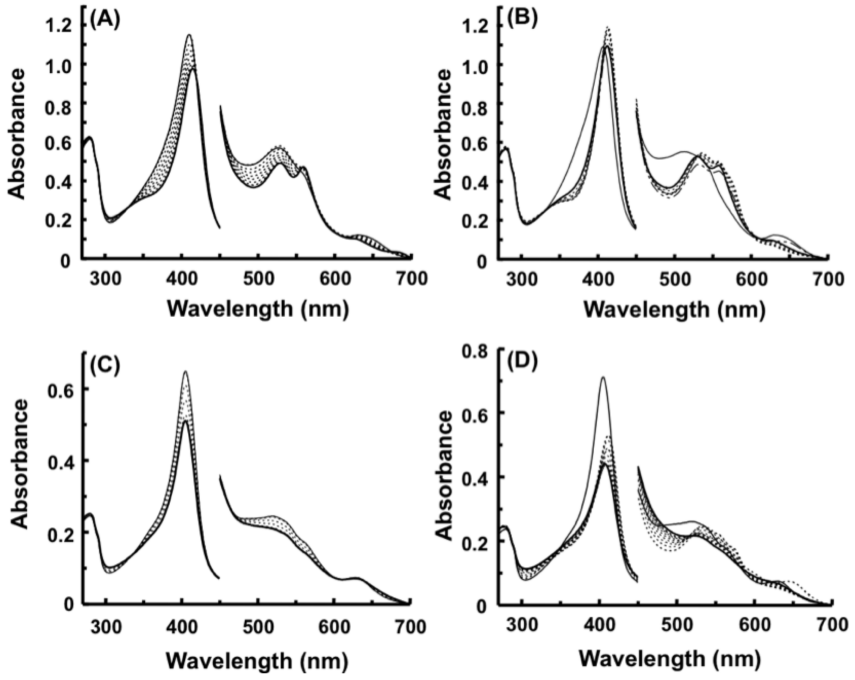

FIGURE 1: Selected electronic spectra collected during the reaction of ferric wild-type APX (A and B) and W41A (C and D) with 14.5 equiv of *t*-BuOOH (A and C) and H_2O_2 (B and D). The intermediate spectra between ferric W41A/wild-type APX (thin solid line) and final spectra of the reaction (thick solid line) are shown as dotted lines. The total reaction time was 15 min. The visible region has been multiplied by a factor of 5. Conditions: sodium phosphate, pH 8.3, μ = 0.1 M, 25.0 °C.

which shows that the ferryl heme is not formed at all on these time scales in solution.

Effect of Reducing Equivalents. We also tested the effect of reducing equivalents, since in the crystal structure experiments (see below) the X-ray beam is a source of reducing equivalents for the heme and it was important to check whether an effect could be seen in solution. We found that addition of ascorbate to W41A and wild-type APX after reaction with H_2O_2 (data not shown), and to wild-type APX on reaction with *t*-BuOOH (Figure 2A), cleanly regenerated ferric heme from Compound II, which is as expected for these peroxidase intermediates. In contrast, addition of ascorbate to W41A after addition of *t*-BuOOH has no effect on the observed spectra under any conditions (Figure 2B). These data together provide confirmation that ferryl heme is not formed on reaction of W41A with *t*-BuOOH, because the presence of a reducing agent has no effect on the spectra and does not regenerate ferric heme as in the other cases above. The possible involvement of reducing agents in the crystallographic experiments is discussed below (see Discussion).

Structural Characterization of the Reaction Product. The structure of ferric W41A has been shown (*22*) to have His42 coordinated to the iron. This His42 is mobile and moves on and off the iron depending on whether or not other ligands or peroxide are present. Here, the crystal structure of W41A soaked in *t*-BuOOH for 15 min was determined. The overall structure and most of the active site were found to be similar to that of ferric W41A, although His42 is no longer bound to the iron and a presumed water molecule (Fe−O distance of 2.1 Å) occupies the position above the heme instead (we note, however, that this distance is not far from what might be expected for a Compound II Fe−OH (1.7−1.8 Å) formed in the crystals from reduction of CII in the beam; see also discussion of Figure 4 below and correlation of solution/structural data in the Discussion).

The electron density around the heme in this structure clearly shows that the heme is cleaved at the α-*meso* position (Figure 3A). The additional density observed directly above the site of heme cleavage (α-*meso*-carbon) was assigned as a *tert*-butyl group, to give the corresponding *tert*-butylbiliverdin species. There was unambiguous electron density for an iron atom in the modified biliverdin species, in close proximity to an active site oxygen atom (Fe−O distance of 2.1 Å). An unambiguous assignment is not possible from the crystallographic data alone, but this distance is consistent with that expected for a water molecule bound to APX (equivalent distance of 2.1 Å in the wild-type APX/ascorbate complex). We note that the α-*meso*-carbon in W41A lies directly below the Ala41 residue in the distal pocket; we interpret this to mean that during the reaction mechanism the *tert*-butyl group of the peroxide likely occupies space in the distal cavity that was previously occupied by Trp41.

Mass Spectrometry. We attempted characterization of the product observed crystallographically using HPLC/mass spectrometry. For wild-type APX and W41A on treatment with H_2O_2, and for wild-type APX on treatment with *t*-BuOOH, a single peak was identified by HPLC analysis of the products (retention time 33 min) which in all three cases was shown by MALDI-Tof mass spectrometry to have a mass of 616 Da, corresponding to free heme, and an isotope distribution that assigns it as containing iron (data not shown). In similar solution experiments on W41A after treatment with *t*-BuOOH we found that the product as observed crystallographically was unstable under various conditions and that mixtures of products were often observed by mass spectrometry (MALDI-Tof and ESI in positive and negative

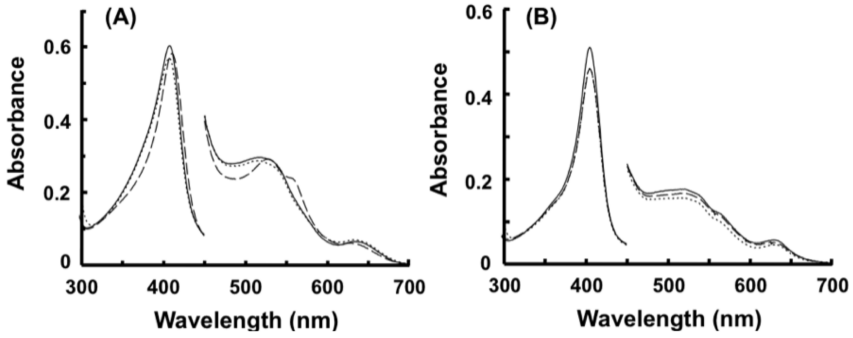

FIGURE 2: Electronic spectra of (A) wild-type APX and (B) ferric W41A prior to addition of *t*-BuOOH (solid line) and immediately after addition of 14.5 equiv of *t*-BuOOH (dashed line). Clear formation of a Compound II species is observed for the wild-type protein but not for W41A. The spectra immediately after subsequent addition of 14.5 equiv of ascorbate to the *t*-BuOOH-treated enzymes are shown as dotted lines in both cases. The visible region has been multiplied by a factor of 5. Conditions: sodium phosphate, pH 8.3, μ = 0.1 M, 25.0 °C.

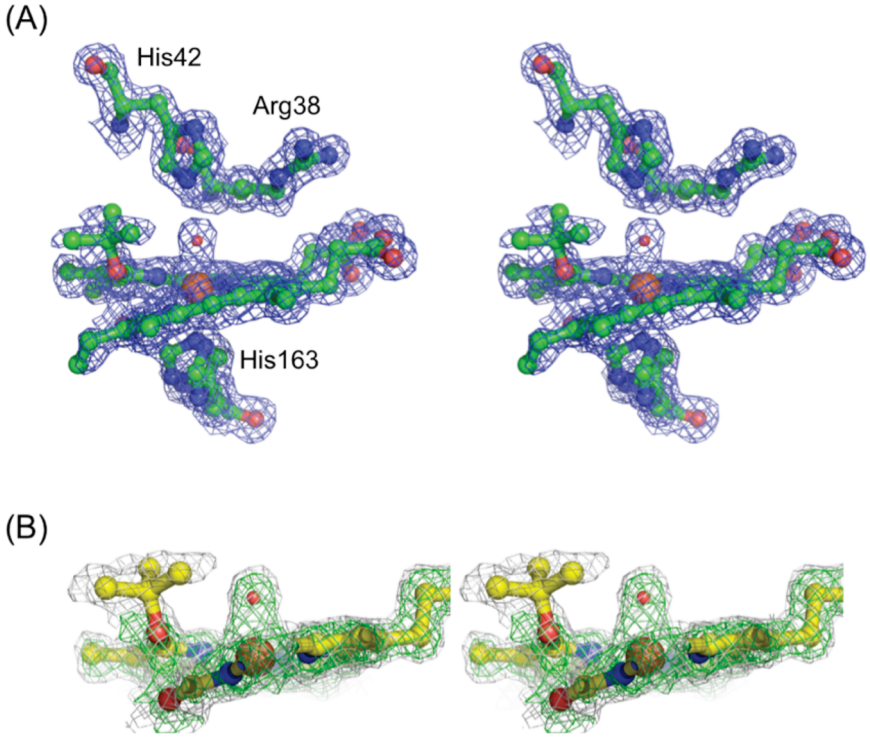

FIGURE 3: (A) Stereoview of the *t*-BuOOH reaction product observed in the crystal. Electron density calculated with coefficients $2F_o - F_c$ and contoured at 1.0σ is shown in blue. The positions of the proximal histidine (His163), the distal histidine (His42), and the conserved arginine (Arg38) are indicated; there are multiple conformations of the proximal histidine, as previously (*22*). An orthogonal view is shown in Supporting Information Figure S2. (B) Stereoview of the W41A/*t*-BuOOH reaction product in the crystal. Electron density calculated using coefficients $F_o - F_c$ and excluding the heme derivative and water atoms is shown at contours of 2σ (gray) and 3σ (green). The lower occupancy of the *tert*-butyl group can be seen clearly.

ion mode). We believe this arises from degradation of the product during sample preparation/handling time scales which were much longer than those used for the crystallographic experiments (15 min). We did, however, repeatedly detect a species (M_r = 583) consistent with formation of biliverdin (M_r = 582) in these MALDI-Tof and electrospray mass spectrometric analyses, which we propose as arising from direct degradation of the product under the (acidic) conditions of these experiments; see Discussion and Scheme 3 (*35*). This would not be inconsistent with the structural data, where the *tert*-butyl group is seen at a lower contour level, and is modeled with a partial occupancy of 0.5, consistent with a mixture of both biliverdin and the *tert*-butyl product in this site (Figure 3B).

Single-Crystal Microspectrophotometry. In parallel experiments, single-crystal microspectrophotometry was also used to monitor the *t*-BuOOH-soaked W41A crystal before and after exposure to the X-ray beam. The spectrum of the soaked crystal at 100 K (Figure 4) collected before data collection was different from that in solution (Figure 1C) with wavelength maxima (λ_{max}/nm = 532 and 559) very close to those observed for the proposed ferric−hydroperoxide intermediates in heme oxygenase (λ_{max}/nm = 421, 530, and 557 (*36*)). Thus, we assign this species as arising from formation of a ferric *tert*-butyl hydroperoxide intermediate (not visible in solution experiments due to it being only transiently stable). After exposure to X-rays, the final spectrum of the crystal (λ_{max}/nm = 532, 563, and 630; Figure 4) was identical

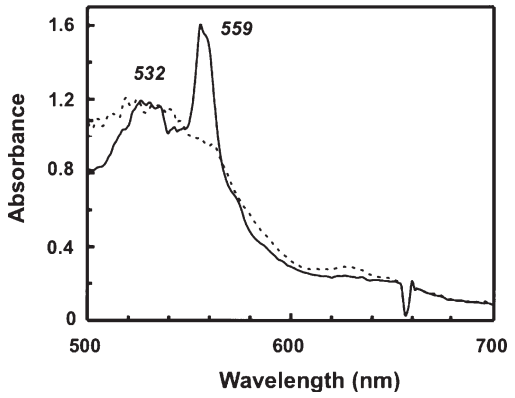

FIGURE 4: Changes in the absorption spectrum (100 K) of a *tert*-BuOOH-soaked crystal of W41A before (solid line) and after (dotted line) exposure to the X-ray beam.

to that observed in the solution experiments on reaction of W41A with *t*-BuOOH (λ_{max}/nm = 532, 563, and 630; Figure 1C above). We take this to mean that the final product in solution and in the crystal is the same but that the intermediates that we can observe at low temperatures are not visible in solution. An alternative suggestion is that the final spectrum in Figure 4 arises from a ferryl species (which would have to mean that formation of ferryl heme is observed only in the crystal (Figure 4) but not in solution). The dotted line in Figure 4 looks similar to what one might expect for a ferryl (Compound I/II) species, but the spectra are not entirely consistent with this interpretation. Compound I of W41A (*22*) shows only one peak at 530 nm (with a shoulder), whereas Figure 4 shows two clear peaks in this region; Compound II of W41A does show two peaks (530, 560 nm), as in Figure 4, but has no peak at 630 nm, which is clearly visible in Figure 4. (We note, however, that high absorbancies in the crystal when collecting single-crystal spectra can lead to spectral abberations.)

DISCUSSION

In this paper, we have presented crystallographic evidence for heme degradation in a peroxidase enzyme on reaction with *t*-BuOOH. Our kinetic data in solution indicate that this degradation of the heme group most likely occurs because formation of a normal peroxidase Compound I intermediate is slowed down to such an extent that its rate of formation becomes uncompetitive. Instead, the reaction diverts through an alternative route not previously observed in a peroxidase enzyme. Although the reaction with *t*-BuOOH is clearly not a physiological process, it is revealing in the sense that it does show us that the HO and peroxidase enzymes likely operate through a similar ferric−peroxide intermediate (as previously suggested (*3*,*7*)) and that their differing reactivities derive from the fate of this intermediate. This is considered in further detail below.

Mechanism of Product Formation. In considering possible mechanisms for product formation, we began from the clear observation that ferryl heme (in the form of Compound I) is not observed on reaction of W41A with *t*-BuOOH. This is consistent with what is known in HO, since ferryl heme is not observed either for HO under normal catalytic conditions. In fact, in cases where ferryl heme is observed for HO (e.g., on reaction with *m*-chloroperoxybenzoic acid and alkyl peroxides such as cumene hydroperoxide, *t*-BuOOH, and EtOOH (*11*,*21*)) formation of verdoheme does not occur (*1*). Further, the microspectrophotometry data lead us to conclude that a ferric−peroxide species is the first intermediate formed on reaction of ferric W41A with *t*-BuOOH. This is consistent with what we know of the reactivity of heme peroxidases in general and with all cited mechanisms for HO in which formation of this same species is an obligate intermediate.

We propose that this ferric−peroxide intermediate is converted first to α-*meso*-hydroxyheme and then to verdoheme by the mechanism shown in Scheme 3A, which is based on the analogous reactions in HO. Thus, HO is known (*11*,*18*,*21*,*37*) to react with O_2 or H_2O_2 (or EtOOH) to carry out α-*meso*-hydroxylation (or ethoxylation) of the heme. Initial mechanistic studies suggested that this reaction proceeds by electrophilic attack on the α-meso-carbon (*4*). The alternative, radical mechanism was regarded as unlikely because it generates HO· as a product of O−O bond cleavage, and this species was thought to be too nonspecific in its reactivity to account for the regioselectivity of the HO reaction. More recently, however, there is evidence from theoretical and experimental work that a radical mechanism might, in fact, be operational for HO (*38*−*45*) because homolytic cleavage of the peroxide O−O bond has a lower energy barrier than the corresponding electrophilic mechanism so that the HO· thus produced selectively targets the correct *meso*-carbon of the heme. Accordingly (Scheme 3A), we propose that initial homolytic cleavage of the O−O bond (Scheme 3A, step ii) generates an intermediate radical species in which the *tert*-butoxy group has added to the α-pyrrole carbon. Oxidation by Fe(IV) (step iii) gives a cationic intermediate which can undergo nucleophilic attack by water (step iv). Subsequent loss of *t*-BuOH (step v) and formation of α-*meso*-hydroxyheme is then followed by conversion to verdoheme as an intermediate (dotted arrow, step vi), and this last step is proposed to occur as an O_2-dependent process as in HO (*1*).

The differing regioselectivity between the first step in this proposed mechanism with that observed for HO may be due to the steric bulk of the *tert*-butyl group. We believe that in W41A the *tert*-butyl group is positioned in an orientation that directs it toward both the α-*meso*-carbon and the α-pyrrole carbon as it is likely to occupy the space that was previously occupied by Trp41 which lies above these two carbon atoms in the wild-type enzyme. Our crystal structure (*22*) for the NO-bound complex of W41A supports this idea because the bound NO adopts two conformations in the active site, rather than one as in the wild-type protein, with the second binding orientation orienting the ligand toward Ala41 and above the α-*meso* and α-pyrrole carbons.

We envisage two possible routes for conversion of verdoheme to the observed product (Scheme 3B). The first (route i) is conceptually more straightforward and involves nucleophilic addition of *t*-BuOH (as a byproduct of the first step) to the α-pyrrole carbon of verdoheme to generate an intermediate that can undergo subsequent

Scheme 3: Proposed Mechanism of the Reaction. (A) Initial Reaction of Ferric W41A with *t*-BuOOH. (B) Possible Routes for Product Formation, Showing the Final Product Which Is Consistent with X-ray Data Shown in Figure 3. (C) Possible Mechanism for Decomposition of the Product[a]

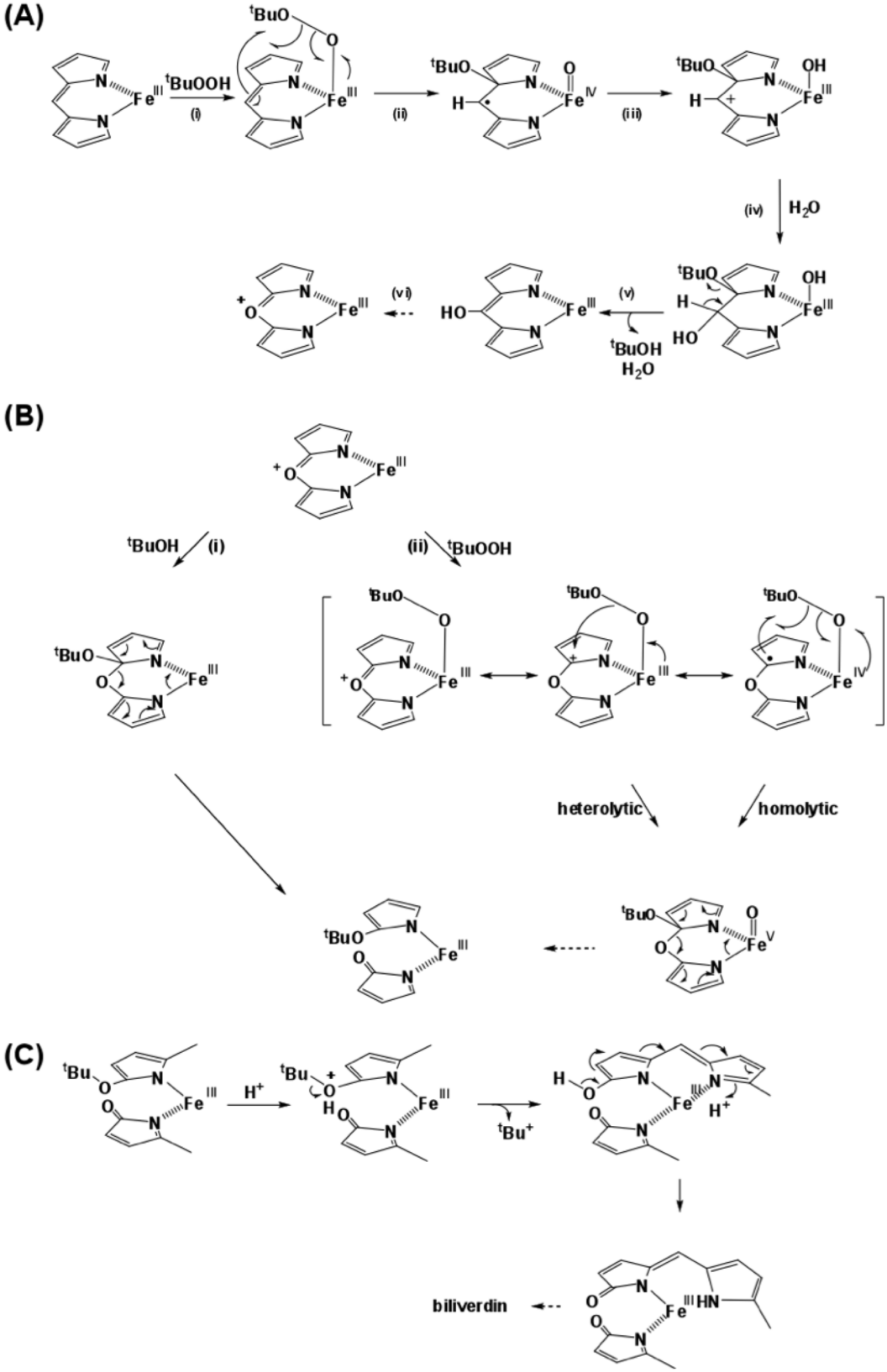

[a] Further details of the individual steps are given in the Discussion.

C−O bond cleavage to give product. The second pathway (route ii) is analogous to the proposed mechanism for the conversion of verdoheme to biliverdin by HO. This conversion was originally (*1*,*11*) thought not to be catalyzed by peroxide, but it is now known (*19*,*20*) that this can indeed occur by reaction of *ferrous* verdoheme with peroxide, formation of a ferrous−peroxide bound intermediate, and heterolytic O−O bond cleavage to give a two-electron oxidized ferryl (Fe^{IV}) heme. Indeed, this mechanism has been used to explain (*20*) the reactivity of HO with MeOOH in which a linear tetrapyrrole product, analogous to our observed product (*t*-Bu replaced by Me; no Fe), resulting from addition of a methoxy group to the α-pyrrole carbon, was observed. Applying a similar mechanism to W41A, initial reaction of ferric−verdoheme with excess *t*-BuOOH (Scheme 3B, route ii) would generate an intermediate that could react via either a heterolytic (as proposed for HO) or homolytic mechanism, as shown in Scheme 3B. However, in contrast to HO, formation of ferrous heme is not possible in our system, at least in solution (but see below, however), because no reducing equivalents are present: both mechanisms would therefore need to invoke formation, formally, of a transient Fe^{V}=O species. We also note that the conversion of verdoheme to biliverdin was found not to occur with ferric verdoheme (*11*,*17*,*46*), which argues against the corresponding mechanism in the W41A/*t*-BuOOH reaction. Therefore, although we cannot rule out route ii, we conclude that this pathway is likely to be unfavorable and thus favor the more straightforward route I in solution.

Correlation between Solution and Structural Data. The situation might be slightly different in the solid state from that observed in solution since exposure to the X-ray source generates reducing equivalents which might allow formation of ferrous verdoheme, so that in the crystallographic experiments product formation might more likely proceed through the mechanism shown in route ii but using ferrous verdoheme (as for HO (*19*,*20*)) instead of ferric verdoheme as shown in Scheme 3B. In fact, if this were the dominant mechanism in the crystal, it would account for the more clear-cut formation of product in the crystallographic experiments compared to that in solution, since the requisite Fe^{V}=O intermediate is quite clearly not observed as an intermediate in solution and characterization of the products is more ambiguous than for the crystallographic experiments. Regardless of the precise mechanism of formation, the final product, as shown in Scheme 3B, is likely to be unstable under acidic conditions and would decompose to biliverdin according to Scheme 3C. This would explain why we have been unable to observe this product in solution or by mass spectrometry (under acidic conditions) and why biliverdin was detected in mass spectra under various solution conditions.

Conclusions. In conclusion, we have presented evidence for heme oxygenase activity in the W41A variant of ascorbate peroxidase on reaction with *t*-BuOOH. By comparison with the wild-type enzyme and with reactions with hydrogen peroxide, it appears that the origin of this activity is the failure of the W41A variant to form the expected Compound I intermediate on reaction with *t*-BuOOH. These observations are consistent with the idea that the heme oxygenase and peroxidase enzymes use a common reaction intermediate, a ferric−hydroperoxide species, and that the specific reactivities of these two enzymes are differentiated by diversion of the mechanism through one of two mutually exclusive reaction pathways.

ACKNOWLEDGMENT

We thank J. McGeehan for assistance at ID14-2, J. Schawbe for collection of crystallographic data, and L. Fairall for assistance with graphics and crystallographic work, S. Ashra and A. Bottril for assistance with mass spectrometry, and P. Ortiz de Montellano for suggestions on possible reaction mechanisms.

SUPPORTING INFORMATION AVAILABLE

Reactions of wild-type APX and W41A with H_2O_2 and *t*-BuOOH (Figure S1) and a stereoview of the *t*-BuOOH reaction product observed in the crystal (Figure S2). This material is available free of charge via the Internet at http://pubs.acs.org.

REFERENCES

1. Ortiz de Montellano, P. R. (1998) Heme oxygenase mechanism: evidence for an electrophilic, ferric peroxide species. *Acc. Chem. Res. 31*, 543–549.
2. Colas, C., and Ortiz de Montellano, P. R. (2003) Autocatalytic radical reactions in physiological prosthetic heme modification. *Chem. Rev. 103*, 2305–2332.
3. Ortiz de Montellano, P. R. (2000) The mechanism of heme oxygenase. *Curr. Opin. Chem. Biol. 4*, 221–227.
4. Ortiz de Montellano, P. R., and Wilks, A. (2001) Heme oxygenase structure and mechanism. *Adv. Inorg. Chem. 51*, 359–407.
5. Sono, M., Roach, M. P., Coulter, E. D., and Dawson, J. H. (1996) Heme-containing oxygenase. *Chem. Rev. 96*, 2841–2887.
6. Yoshida, T., and Migita, C. T. (2000) Mechanism of heme degradation by heme oxygenase. *J. Inorg. Biochem. 82*, 33–41.
7. Unno, M., Matsui, T., and Ikeda-Saito, M. (2007) Structure and catalytic mechanism of heme oxygenase. *Nat. Prod. Rep. 24*, 553–570.
8. Verma, A., Hirsch, D. L., Glatt, C. E., Ronnet, G. V., and Snyder, S. H. (1993) Carbon monoxide: a putative neural messenger. *Science 259*, 381–384.
9. Nathanson, J. A., Scavone, C., Scanlon, C., and McKee, M. (1995) The cellular cellular Na^+ pump as a site of action for carbon monoxide and glutamate: a mechanism for long-term modulation of cellular activity. *Neuron 14*, 781–794.
10. Zakhary, R., Gaine, S. P., Dinerman, J. L., Ruat, M., Flavahan, N. A., and Synyder, S. H. (1996) Heme oxygenase 2: endothelial and neuronal localization and role in endothelium-dependent relaxation. *Proc. Natl. Acad. Sci. U.S.A. 93*, 795–798.
11. Wilks, A., and Ortiz de Montellano, P. R. (1993) Rat liver heme oxygenase. High level expression of a truncated soluble form and nature of the meso-hydroxylating species. *J. Biol. Chem. 268*, 22357–22362.
12. Matera, K. M., Takahashi, S., Fujii, H., Zhou, H., Ishikawa, K., Yoshimura, T., Rousseau, D. L., Yoshida, T., and Ikeda-Saito, M. (1996) Oxygen and one reducing equivalent are both required for the conversion of hydroxyhemin to verdoheme in heme oxygenase. *J. Biol. Chem. 271*, 6618–6624.
13. Wilks, A., and Moenne-Loccoz, P. (2000) Identification of the proximal ligand His-20 in heme oxygenase (Hmu O) from *Corynebacterium diphtheriae*. *J. Biol. Chem. 275*, 11686–11692.
14. Chu, C. G., Katakura, K., Zhang, X., Yoshida, T., and Ikeda-Saito, M. (1999) Heme degradation as catalyzed by a recombinant bacterial heme oxygenase (Hmu O) from *Corynebacterium diphtheriae*. *J. Biol. Chem. 274*, 21319–21325.
15. Chu, C. G., Tomita, T., Sonnichsen, F. D., Yoshida, T., and Ikeda-Saito, M. (1999) The heme complex of Hmu O, a bacterial heme degradation enzyme from *Corynebacterium diphtheriae*. *J. Biol. Chem. 274*, 24490–24496.

16. Chu, C. G., Katakura, K., Tomita, T., Zhang, X., Sun, D., Sato, M., Sasahara, M., Kayama, T., Ikeda-Saito, M., and Yoshida, T. (2000) Histidine 20, the crucial proximal axial heme ligand of bacterial heme oxygenase Hmu O from *Corynebacterium diphtheriae*. *J. Biol. Chem. 275*, 17494–17500.
17. Liu, Y., Moenne-Loccoz, P., Loehr, T. M., and Ortiz de Montellano, P. R. (1997) Heme oxygenase-1, intermediates in verdoheme formation and the requirement for reduction equivalents. *J. Biol. Chem. 272*, 6909–6917.
18. Ishikawa, K., Takaeuchi, N., Takahashi, S., Matera, K. M., Sato, M., Shibahara, S., Rousseau, D. L., Ikeda-Saito, M., and Yoshida, T. (1995) Heme oxygenase-2. *J. Biol. Chem. 270*, 6345–6350.
19. Matsui, T., Nakajima, A., Fujii, H., Matera, K. M., Migita, C. T., Yoshida, T., and Ikeda-Saito, M. (2005) O_2- and H_2O_2-dependent verdoheme degradation by heme oxygenase: reaction mechanisms and potential physiological roles of the dual pathway degradation. *J. Biol. Chem. 280*, 36833–36840.
20. Matsui, T., Omori, K., Jin, H., and Ikeda-Saito, M. (2008) Alkyl peroxides reveal the ring opening mechanism of verdoheme catalyzed by heme oxygenase. *J. Am. Chem. Soc. 130*, 4220–4221.
21. Wilks, A., Torpey, J., and Ortiz de Montellano, P. R. (1994) Heme oxygenase (HO-1). Evidence for electrophilic oxygen addition to the porphyrin ring in the formation of alpha-meso-hydroxyheme. *J. Biol. Chem. 269*, 29553–29556.
22. Badyal, S. K., Joyce, M. G., Sharp, K. H., Seward, H. E., Mewies, M., Basran, J., Macdonald, I. K., Moody, P. C. E., and Raven, E. L. (2006) Conformational mobility in the active site of a heme peroxidase. *J. Biol. Chem. 281*, 24512–24520.
23. Asada, K. (1984) Chloroplasts: formation of active oxygen and its scavenging. *Methods Enzymol. 105*, 422–429.
24. Nelson, D. P., and Kiesow, L. A. (1972) Enthalpy of decomposition of hydrogen peroxide by catalase at 25 °C. *Anal. Biochem. 49*, 474–478.
25. Metcalfe, C. L., Ott, M., Patel, N., Singh, K., Mistry, S. C., Goff, H. M., and Raven, E. L. (2004) Autocatalytic formation of green heme: evidence for H_2O_2-dependent formation of a covalent methionine-heme linkage in ascorbate peroxidase. *J. Am. Chem. Soc. 126*, 16242–16248.
26. Jones, D. K., Dalton, D. A., Rosell, F. I., and Raven, E. L. (1998) Class I heme peroxidases: characterisation of soybean ascorbate peroxidase. *Arch. Biochem. Biophys. 360*, 173–178.
27. Sharp, K. H., Mewies, M., Moody, P. C. E., and Raven, E. L. (2003) Crystal structure of the ascorbate peroxidase-ascorbate comples. *Nat. Struct. Biol. 10*, 303–307.
28. Leslie, A. G. W. (1992) Recent changes to the MOSFLM package for processing film and image plate data. *Jt. CCP4 + ESF-EAMCB Newsl. Protein Crystallogr. 26*, 134–135.
29. Collaborative Computational Project Number 4 (1994) The CCP4 suite: programs for protein crystallography. *Acta Crystallogr., Sect. D 50*, 760–763.
30. Lad, L., Friedman, J., Li, H., Bhaskar, B., Ortiz de Montellano, P. R., and Poulos, T. L. (2004) Crystal structure of human heme oxygenase-1 in a complex with biliverdin. *Biochemistry 43*, 3793–3801.
31. Murshudov, G. N., Vagin, A., A., and Dodson, E. J. (1997) Refinement of macromolecular structures by the maximum-likelihood method. *Acta Crystallogr., Sect. D 53*, 240–255.
32. Emsley, P., and Cowtan, K. (2004) *Coot*: model-building tools for molecular graphics. *Acta Crystallogr., Sect. D 60*, 2126–2132.
33. Fujii, H., Zhang, X., Tomita, T., Ikeda-Saito, M., and Yoshida, T. (2001) A role for highly conserved carboxylate, aspartate-140, in oxygen activation and heme degradation by heme oxygenase-1. *J. Am. Chem. Soc. 123*, 6475–6484.
34. Lad, L., Mewies, M., and Raven, E. L. (2002) Substrate binding and catalytic mechanism in ascorbate peroxidase: evidence for two ascorbate binding sites. *Biochemistry 41*, 13774–13781.
35. De Matteis, F., Lord, G. A., Kee Lim, C., and Pons, N. (2006) Bilirubin degradation by uncoupled cytochrome P450. *Rapid Commun. Mass Spectrom. 20*, 1209–1217.
36. Denisov, I. G., Ikeda-Saito, M., Yoshida, T., and Sligar, S. G. (2002) Cryogenic absorption spectra of hydroperoxo-ferric heme oxygenase, the active intermediate of enzymatic heme oxygenation. *FEBS Lett. 532*, 203–206.
37. Yoshida, T., Noguchi, M., and Kikuchi, G. J. (1980) Oxygenated form of heme·heme oxygenase complex and requirement for second electron to initiate heme degradation from the oxygenated complex. J. Biol. Chem. 255, 4418–4420.
38. Kumar, P., de Visser, S. P., and Shaik, S. (2005) Theory favors a stepwise mechanism of porphyrin degradation by a ferric hydroperoxide model of the active species of heme oxygenase. *J. Am. Chem. Soc. 127*, 8204–8213.
39. Wojciechowski, G., and Ortiz de Montellano, P. R. (2007) Radical energies and the regiochemistry of addition to heme groups. methylperoxy and nitrite radical additions to the heme of horseradish peroxidase. *J. Am. Chem. Soc. 129*, 1663–1672.
40. deVisser, S. P., Shaik, S., Sharma, P. K., Kumar, D., and Thiel, W (2003) Active species of horseradish peroxidase (HRP) and cytochrome P450: two electronic chameleons. *J. Am. Chem. Soc. 125*, 15779–15788.
41. Kamachi, T., and Yoshizawa, K. (2005) Water-assisted oxo mechanism for heme metabolism. *J. Am. Chem. Soc. 127*, 10686–10692.
42. Chen, H., Moreau, Y., Derat, E., and Shaik, S. (2008) Quantum mechanical/molecular mechanical study of mechanisms of heme degradation by the enzyme heme oxygenase: the strategic function of the water cluster. *J. Am. Chem. Soc. 130*, 1953–1965.
43. Sharma, P., Kevorkiants, R., de Visser, S. P., Kumar, D., and Shaik, S. (2004) Porphyrin traps its terminator! Concerted and stepwise porphyrin degradation mechanisms induced by heme-oxygenase and cytochrome P450. *Angew. Chem., Int. Ed. 43*, 1129–1132.
44. Kamachi, T., Shestakov, A. F., and Yoshizawa, K. (2004) How heme metabolism occurs in heme oxygenase: computational study of oxygen-donation ability of the oxo and hydroperoxo species. *J. Am. Chem. Soc. 126*, 3672–3673.
45. Rivera, M., Caigen, G. A., Astashkin, A. V., Raitimring, A. M., Shokhireva, T. K., and Walker, F. A. (2002) Models of the low-spin iron(III) hydroperoxide intermediate of heme oxygenase: magnetic resonance evidence for thermodynamic stabilization of the dxy electronic state at ambient temperatures. *J. Am. Chem. Soc. 124*, 6077–6089.
46. Liu, Y., and Ortiz de Montellano, P. R. (2000) Reaction intermediates and single turnover rate constants for the oxidation of heme by human heme oxygenase-1. *J. Biol. Chem. 275*, 5297–5307.